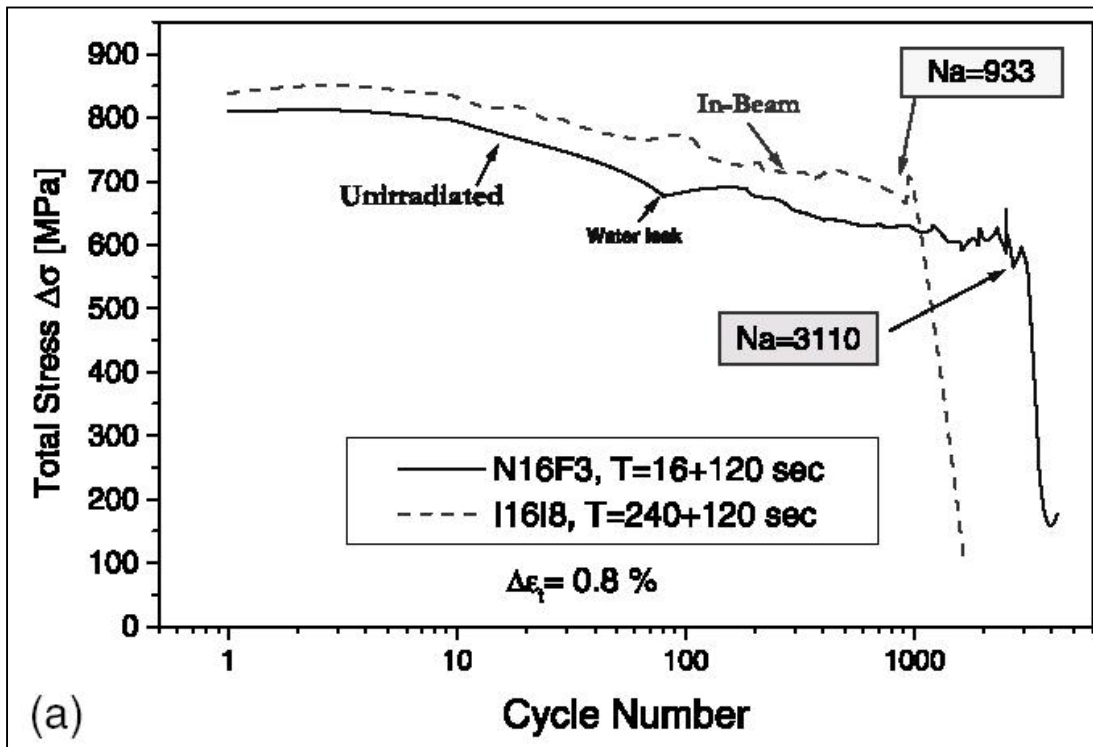**Material:** Ferritic Steel: F82H
Property: Total Stress Range vs. Cycle Number
Condition: Proton Irradiation
Data: Experimental
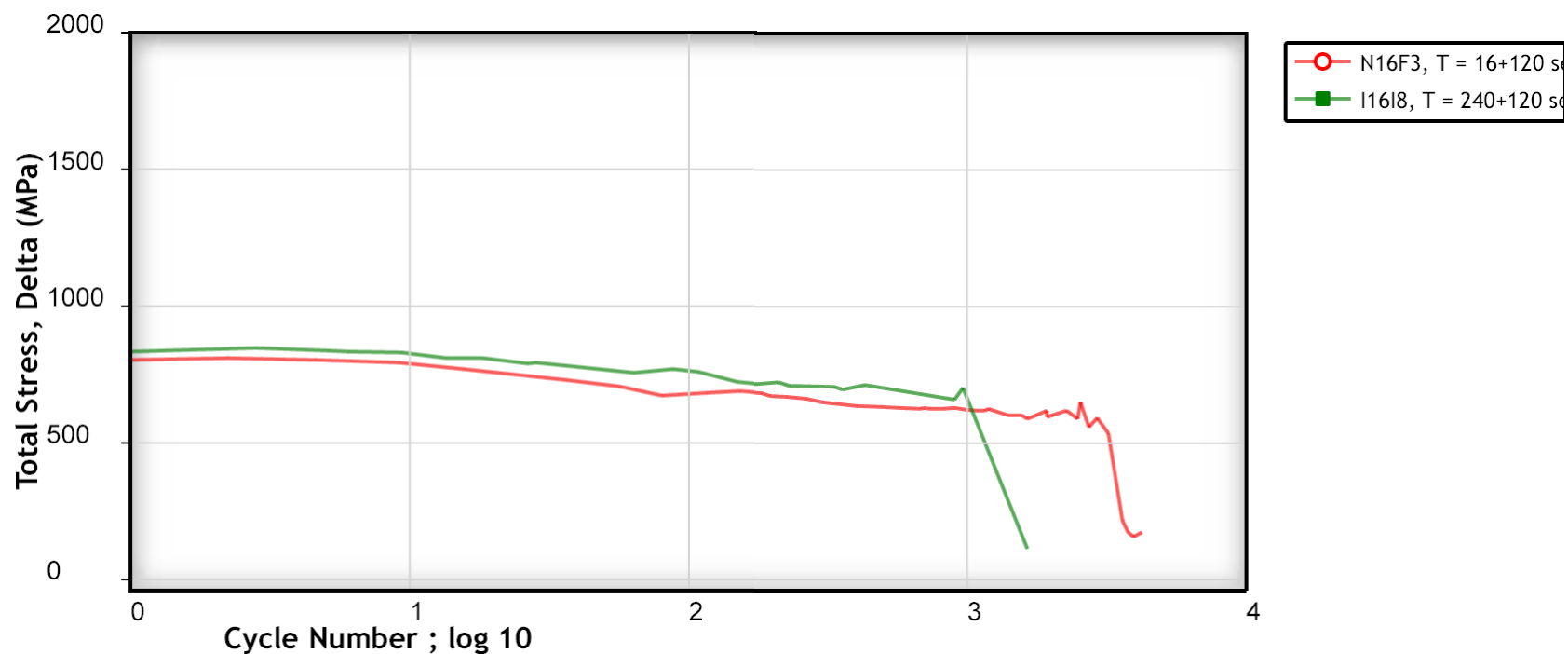
Title of paper (or report) this figure appeared in:
High Strain Fatigue Properties of F82H Ferritic-Martensitic Steel Under Proton Irradiation

Author of paper or graph:
P. Marmy, B.M. Oliver

Caption:
Total stress range $\Delta\sigma$ as a function of the cycle number for the specimen I16I8, fatigued with 2 min tensile hold times.

Total stress range Δσ as a function of the cycle number for the specimen I16I8, fatigued with 2 min tensile hold times (Δε_t = 0.8%).

View Data   Author Comments

Plot Format:

  Y-Scale: ⦿ linear ○ log ○ ln
  X-Scale: ○ linear ⦿ log ○ ln

High strain fatigue properties of F82H ferritic–martensitic steel under proton irradiation

P. Marmy [a,*], B.M. Oliver [b]

[a] *Centre de Recherche en Physique des Plasmas, Technologie de la Fusion, Association Euratom – Confédération Suisse, Ecole Polytechnique Fédérale de Lausanne, Villigen-PSI CH-5232, Switzerland*
[b] *Pacific Northwest National Laboratory, P.O. Box 999, Richland, WA 99352, USA*

Abstract

During the up and down cycles of a fusion reactor, the first wall is exposed concomitantly to a flux of energetic neutrons that generates radiation defects and to a thermal flux that induces thermal stresses. The resulting strains may exceed the elastic limit and induce plastic deformation in the material. A similar situation occurs in the window of a spallation liquid source target and results in the same type of damage. This particular loading has been simulated in F82H ferritic–martensitic steel, using a device allowing a fatigue test to be carried out during irradiation with 590 MeV protons. All fatigue tests were carried out in a strain controlled test at strain levels around 0.8% and at 300 °C. Two different signals have been used: a fully symmetrical triangle wave signal ($R = -1$) and a triangle ramp with 2 min tension holds. The fatigue was investigated under three different conditions: unirradiated, irradiated and post-irradiation tested, and finally *in-beam* tested. The main result is that the *in-beam* tested specimens have the lowest life as compared to the post-irradiation tested specimen and unirradiated specimen. Hydrogen is suspected to be the main contributor to the observed embrittlement.
© 2003 Elsevier Science B.V. All rights reserved.

1. Introduction

The F82H steel is a first generation alloy of the so called reduced activation ferritic–martensitic steel family. These steels are among the promising materials for building the first wall components of a fusion reactor. Their interesting physical characteristics are high strength and good heat conduction. They have a relatively low ductile to brittle transition temperature and have minimal swelling under irradiation. In the first wall components of a future thermonuclear reactor, these materials would be exposed to concurrent thermal and neutron loads. This loading would probably induce stresses beyond the elastic limit during the start up and the shut down of the reactor. Due to the pulsed opera-

tion of tokamak devices, one of the important issues concerning the materials will almost certainly be fatigue.

Considering the conceptual design of future spallation neutron sources [1,2], the window of the target liquid metal container will be exposed to a similar loading situation, in which cyclic stresses occur during the irradiation. The cyclic stresses may be somewhat lower and the frequency much higher. Nevertheless, the main issue remains the lack of knowledge about the damaging mechanisms that may occur when the material is stressed under irradiation. This is a common problem for both a fusion first wall and a spallation source target window. Certainly the production of He (40 appm/dpa in SNS, for example) and H (500 appm/dpa in SNS), as well as many other spallation products during irradiation could lead to unforeseen and unknown damage mechanisms, if the bulk material is under stress during the irradiation.

The only results available today for comparison are from fission neutron in-pile experiments or from light

---

* Corresponding author. Tel.: +41-56 310 29 32; fax: +41-56 310 45 29.
E-mail address: pierre.marmy@psi.ch (P. Marmy).

ion in situ irradiations. In-pile fatigue tests carried out in a fission reactor do not show drastic effects on the low cycle fatigue performance of austenitic steels [3,4]. Tested under stress control (580 MPa, corresponding to a relatively high strain), the fatigue life at 250 °C was nearly the same as in the unirradiated case. No or little irradiation hardening occurred. In situ crack growth experiments using thin 316 stainless steel notched specimens irradiated with 18 MeV protons have shown only little effects. The crack growth rate observed at temperatures between 100 and 500 °C was smaller under simultaneous irradiation and cyclic stresses [5,6]. Torsion creep fatigue tests have also been performed in 316L SS at 400 °C under irradiation with 19 MeV deuterons. The continuous cycling tests conducted under irradiation lie within the scatter band of the thermal control tests [7]. Irradiation hardening is absent, or if present is rapidly annealed. For tests with hold times, there is a significant reduction of the fatigue life. The effect is attributed to irradiation induced hardening [7,8].

In-beam fatigue tests in MANET steels have been performed with 104 MeV particles, at 250 and 420 °C [9,10]. In the cycle-to-failure plot, the *in-beam* specimens fall in the scatterband of the unirradiated specimens. They have a longer life than the post-irradiation tested specimens. A similar dislocation and helium bubble substructure is observed in the irradiated specimens. The bubbles are slightly coarser in the case of the *in-beam* specimens. *In-beam* fatigue slows down the cyclic softening and irradiation hardening occurs after a high number of cycles. The irradiation hardening is attributed to the helium substructure which impedes the motion of the dislocations.

A device allowing an isothermal fatigue test to be carried out during irradiation with 590 MeV protons has been developed at PSI (Paul Scherrer Institute, Villigen, Switzerland) to simulate the particular loading of the first wall of a fusion reactor [11]. Five hundred and ninety mega electron volt protons are produced in the PSI accelerator, and they provide a good simulation of the 14 MeV fusion neutrons. They produce helium and hydrogen by spallation reactions at levels higher than those of high energy fusion neutrons and with similar displacement damage substructure [12]. In steel, the predicted amounts of helium and hydrogen generated are 195 and 956 appm per dpa [13], respectively. A series of in situ fatigue tests has already been produced in the MANET II steel [11,14,15]. The results agree in general with those mentioned above with the following difference: In the MANET steel, when using high energy protons as the irradiating particle, the life was generally shorter as compared to the unirradiated case and often also shorter than the post-irradiated specimens. TEM and SEM microscopy was undertaken to try to understand the observed effects on the mechanical properties. The damage mechanism causing the reduction of life, in the absence of irradiation hardening, could not be identified.

This work is a continuation of the previous work using the F82H ferritic–martensitic steel.

2. Experimental

2.1. Material and specimens

The F82H material used in this research is an IEA-modified Japanese F82H steel, heat number 9753, rolled to a 25 mm plate. The chemical analysis is given in Table 1.

The specimens were given the following heat treatment: they were first austenitized for 38 min at 1040 °C and then air cooled. Subsequently the specimens were annealed at 750 °C for 2 h and then air cooled. The microstructure consists of martensite laths of approximately 1 μm wide and can attain about 5 μm in length. The lath boundaries are decorated with $M_{23}C_6$ carbides. The carbides are present also on the primary austenite grain boundaries and in the interior of the laths. The carbides are composed of Cr, Fe and W, and it appears that the bulk carbides are coherent with the matrix. The laths contain a high density of predominantly screw dislocations [16].

In-beam testing was carried out using tubular specimens specially designed for the proton experiment, having a cross-section of 2.7×3.4 mm and a gauge length of 5.5 mm. Comparison tests have been carried out using classical subsize specimens with identical gauge dimensions. The specimens were cut in the rolling direction. Details and drawings of the specimens can be seen in [11,17].

2.2. Mechanical tests

Mechanical tests in unirradiated material were performed using an electromechanical testing machine equipped with a vacuum furnace. The pressure in the chamber was about 10^{-6} mbar. In order to control the

Table 1
The chemical composition of modified F82H, heat 9753

C	Si	Mn	Cr	V	Ni	W
0.09	0.07	0.1	7.84	0.19	0.02	1.98

irradiation temperature, the *in-beam* specimens were actively cooled using a flow of pressurized helium (30 bars, [11]). The outside of the specimen is in a vacuum. All mechanical tests presented in this work were performed at 300 °C.

Two types of wave signals have been used to control the strain: triangle ramps ($R = -1$) and triangle ramps with tensile holds of 2 min. The strain is measured with an extensometer directly mounted onto the *in-beam* specimen. The mechanical test parameters are given in Table 2 for all specimens. Except for specimens N16F3 and I16I8, which were held in tension for 2 min, the specimens were tested under continuous fatigue. The fatigue tests were carried out up to the failure of the specimen which corresponded to the separation of the specimen into two halves (N_f). The end of life criteria used to compare the lives was when the main crack penetrated through the specimen wall ($N = N_a$). This point was clearly indicated in the *in-beam* experiment by a failure of the vacuum produced by the out flowing helium. To this point corresponded an inflexion point in the bottom part of the strain–stress hysteresis, which is also clearly marked in the classical fatigue specimen, although no helium pressure is present in the specimen. After the test was interrupted by the vacuum failure, the test was continued without helium, in a vacuum, at an equilibrium temperature of about 40 °C. N_a is considered a better parameter for comparison since at cycles higher than N_a, the mechanical conditions are modified. Depending on the orientation of the main crack, the number of cycles to failure is also affected by a larger dispersion. Scanning electron microscopy was done with

a Zeiss DSM 962, equipped with a tungsten cathode, operating at a maximum voltage of 30 keV.

2.3. Irradiation parameters

The 590 MeV proton beam had a spatial shape corresponding to a gaussian distribution with elliptical diameters of $4\sigma_x = 6$ mm and $4\sigma_y = 3$ mm. A wobbler moved the beam ±2.5 mm with a frequency of 1.8 Hz, to achieve a constant dose deposition along the gauge length. The beam intensity was 16–18 µA. Such a proton beam results in a power input of approximately 4000 W/ cm^3 in steel. This heat is evacuated into the cooling helium ($T_{He} = 275$ °C) by heat convection through a temperature gradient of approximately 25 °C. The irradiation temperature was 300 °C for all specimens. The dose was estimated from the beam-time integral and from dosimetry measurements using the Mn-54 production isotope. The mean parameters obtained during the experiments are summarized in Table 3.

3. Results

3.1. Mechanical tests

3.1.1. General behaviour

The different test and irradiation parameters imposed on the specimens have a clear effect on the number of cycles to end of life, N_a. This is shown in Table 2 and Fig. 1. The specimen with the longest life is the unirradiated

Table 2
The mechanical tests parameters imposed on the specimens and the number of cycles to failure, N_a and N_f, obtained

	N16F2	I16I5	I16I7	I16I9	I16I11	N16F3	I16I8
$\Delta\varepsilon$ total [%]	0.8	0.7	0.8	0.8	0.8	0.8	0.8
T [s]	16	240	240	40	90	16 + 120	240 + 120
$\dot{\varepsilon}$ [s^{-1}]	0.001	5.8×10^{-5}	6.7×10^{-5}	4×10^{-4}	1.78×10^{-4}	0.001	6.7×10^{-5}
N_a	3080	2064	1900	2550	2028	3110	933
N_f	3595	2819	2358	3095	3500	4212	1644

The temperature was 300 °C in all tests. Specimens N16F2 and N16F3 were tested in the unirradiated condition and specimen I16I9 was tested after irradiation. Two min tensile hold-times were imposed on specimens N16F3 and I16I8. Specimen I16I8 with 2 min tensile hold-times had the shortest life.

Table 3
The irradiation parameters achieved in the 590 MeV proton irradiation

	I16I5	I16I7	I16I8	I16I9	I16I11
Dose rate: $\dot{D}$ [dpa/s]	3.3×10^{-7}	5.4×10^{-7}	5.4×10^{-7}	4×10^{-7}	5.2×10^{-7}
Damage ratio: $\dot{D}/\dot{\varepsilon}$ [dpa]	5.69×10^{-3}	8.06×10^{-3}	8.06×10^{-3}	–	2.92×10^{-3}
Accumulated dose: D [dpa]	0.2	0.3	0.23	0.31	0.18

I16I9 was tested after irradiation. Predicted helium production ratio: 195 appm/dpa.
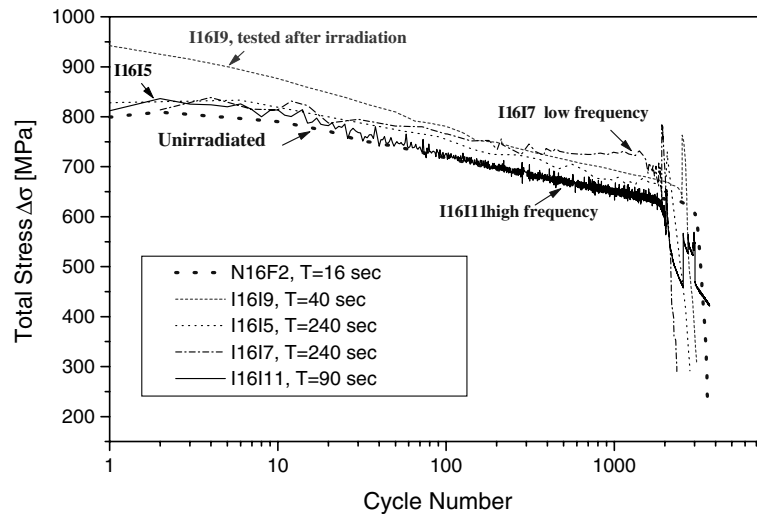
Fig. 1. Total stress range $\Delta\sigma$ as a function of the cycle number for the unirradiated, the post-irradiation tested, and the *in-beam* specimens. The test and irradiation parameters are given in Tables 2 and 3. Test temperature and irradiation temperature: 300 °C. Material: F82H.
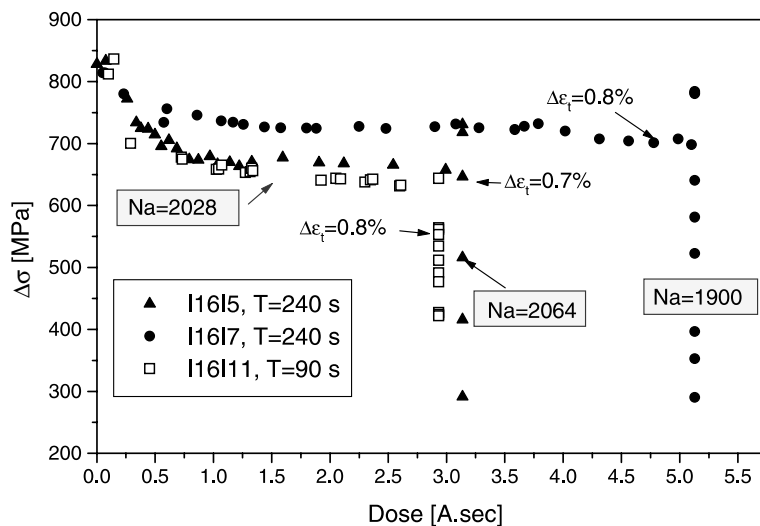

Fig. 2. Total stress range $\Delta\sigma$ as a function of the accumulated dose. N_a is the number of cycles corresponding to the first crack going through the wall. The specimen I16I7, having the higher period of cycle accumulates more dose but fails earlier, as compared to I16I11.

one. I16I9 was irradiated to 0.3 dpa using the in situ device and then fatigue tested after the irradiation at 300 °C in the helium flow. The life was shorter by 17% as compared to the unirradiated specimen. The three *in-beam* experiments shown in Fig. 1 for comparison all have shorter lives than the post-irradiated specimen. The imposed total strain in experiment I16I5 was 0.7%, but 0.8% in the other experiments shown in Fig. 1. Fig. 2 compares the three *in-beam* experiments I16I5, I16I7, and I16I11, as a function of the accumulated dose. The experiments have similar number of cycles. While I16I7 reached a dose that was 30% higher than I16I11, its number of cycles to failure was shorter by 10%. While I16I5 and I16I11 have similar lives, they have non identical imposed strain (0.7% and 0.8%). These figures seem contradictory but in fact they are not because of the different damage ratios [11] indicated in Table 3. Table 2 indicates clearly that the life is shorter when fatigue is imposed concurrently with irradiation by high energy protons.

The softening curves of Fig. 1 show the behavior typical of *in-beam* fatigue [14]. The post-irradiated specimens have the strongest softening. Up to the end of life, the stress level remains above the stress level of the unirradiated specimens. The *in-beam* specimens have the lowest softening rate. Their stress level at end of life is slightly above the stress level of the unirradiated specimen.

3.1.2. Effects of frequency

Fig. 1 also compares two *in-beam* experiments having the same imposed total strain of 0.8% but different fatigue frequencies, as a function of the number of cycles. The post irradiated specimen I16I9 is shown for comparison. I16I7 has a low fatigue frequency ($T = 240$ s, 0.004 Hz) and therefore has a lower softening rate as compared to I16I11 ($T = 90$ s, 0.011 Hz). Correspondingly, the life of I16I7 is shorter than I16I11, which is also in agreement with the damage ratios indicated in Table 3.

The classical irradiation hardening shown by specimen I16I9 ($\Delta\sigma_{irr} = 140$ Mpa) is absent in the *in-beam* specimens, when tested at high frequency. But tested at a low frequency, I16I7 shows some residual irradiation hardening at end of life. Fig. 3 illustrates the effect of imposed mechanical frequency on the resulting total plastic strain. The figure shows that the plastic component of strain is significantly reduced when the frequency is reduced.

3.1.3. Effects of hold-times

Additionally, the introduction of tensile hold-times of 2 min does not affect the endurance (N16F2 and N16F3) in the unirradiated condition. But when the hold time is imposed during the *in-beam* fatigue, then the effect on life is significant (Fig. 4(a)). For practical reasons, the test frequency of the unirradiated specimens has been set higher as compared to the in-beam tested specimens. This should have no effect on the results since thermal-creep effects are not expected at 300 °C, in FM steels. Specimen I16I8 has the shortest life of all specimens. Fig. 4(b) indicates that the plastic strain is smaller during the *in-beam* fatigue. The relaxed stress has been plotted as a function of the number cycles in Fig. 4(c). The stress relaxed during the *in-beam* tension hold is smaller.

3.2. Observations of the fractographs

In general, cracks started at or below the surface and propagated along the tube wall circumference. The appearance of a stable crack propagation phase is shown in Fig. 5(A) for the case of specimen I16I11. Between the fatigue striations, numerous secondary cracks are clearly visible. The cracks have lengths between 3 and 20 μm. The cracks are mainly parallel and separated by a distance of approximately 1–2 μm, and have a distribution similar to the lath boundaries of the martensitic structure. This crack appearance has been found to be typical for all conditions observed in the F82H, irradiated and unirradiated. Fig. 5(B) shows a large secondary crack in the fractograph of specimen I16I9, deformed after irradiation. The same field of tiny microcracks as well as fatigue striations are also visible in the region above the large secondary crack. The region below the secondary crack appears more brittle, is less deformed, and seems
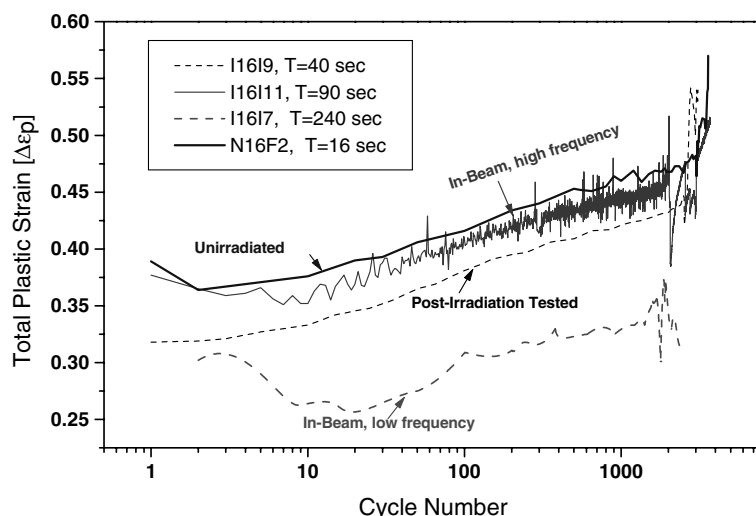

Fig. 3. Total plastic strain $\Delta\varepsilon_p$ as a function of the number of cycles. The *in-beam* specimen tested at low frequency show the smallest total plastic strain.
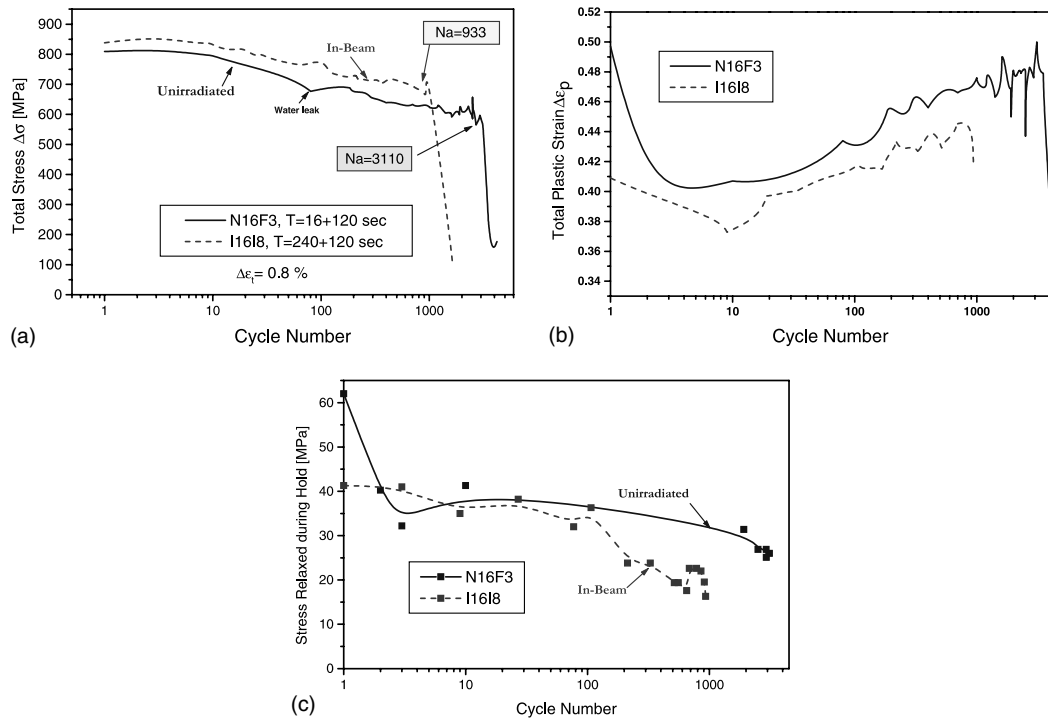
Fig. 4. Total stress range $\Delta\sigma$, total plastic strain $\Delta\varepsilon_p$ and relaxed stress as a function of the cycle number for the specimen I16I8, fatigued with 2 min tensile hold times. The test and irradiation parameters are given in Tables 2 and 3.
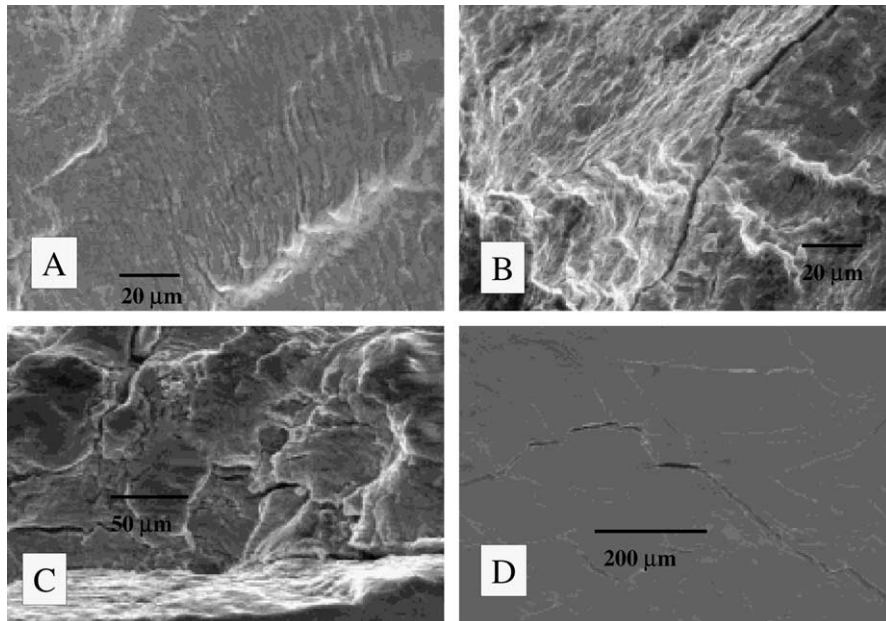

Fig. 5. Fractographs of the *in-beam* specimens. (A) Field of microcracks and striations in the specimen I16I11, (B) large secondary crack in specimen I16I9, (C) intergranular cracks in specimen I16I5 and (D) long intergranular crack in the outside surface of specimen I16I8.

Table 4
Helium and hydrogen concentrations in atomic parts per million for all conditions

Specimen	dpa	Measured hydrogen		Measured helium	
		appm	appm/dpa	appm	appm/dpa
N16I4	–	189	–	–	–
	–	105			
	–	242[a]			
	–	260[a]			
N16I10	–	118	–	–	–
	–	135			
	–	154[b]			
	–	194[b]	–	–	–
I16I5	0.115	616	5357	16.7	145
		754	6557	21.2	184
		86[b]	748		
I16I7	0.271	231	852	36.2	134
		213	786	40.9	151
		87[b]	321		
I16I8	0.184	172	935	15.7	85
		160	870	15.3	83
		292[a]	1587		
	0.217[c]	277[a]	1276[c]		
	0.214[c]	123[ab]	575[c]		
I16I9	0.248	263	1060	35.7	144
		169	681	34.6	140
		85[b]	343		
I16I11	0.112	307	2741	14.0	125
				11.9	106
	0.113[c]	580	5133[c]		
	0.134[c]	66[b]	493[c]		
I16T38	0.454	217	478	57.5	127
		104[b]	229	57.6	127
	0.443[c]	355	801[c]		

N16I4 (deformed 5352 cycles, RT) and N16I10 (as received, RT) are the unirradiated control samples. I16T38 is the irradiated control specimen (not deformed, $T_{irr} = 250$ °C). Dose data are marked with 'c', when the corresponding segment has been measured (see text for more details). All He samples were etched and then acetone cleaned. The hydrogen samples were etched (marked with 'b'), sand blasted (marked with 'a'), or etched and sand blasted (marked with 'ab'), then acetone cleaned.

to belong to grains with a different orientation. Strong intergranular cracking is shown in regions near to the surface of *in-beam* specimen I16I5 in Fig. 5(C). Intergranular cracking was also clearly observed in specimens I16I7 and I16I8. Fig. 5(D) shows a very large intergranular crack on the outside surface of specimen I16I8. In I16I9 and I16I11, intergranular cracking was not clearly observed. Secondary cracks were found on the outside and on the inside surface of the specimens, for all conditions. Their number density was much less than the density of cracks observed in the bulk material.

Quasi-brittle features were observed for all conditions and seem typical for this F82H grade. However, on average, the number of brittle features observed in the *in-beam* specimens, like facets, intergranular cracks,

quasi-cleaved areas, low deformed surfaces, was higher. Specimen I16I8 showed the highest number of these features.

3.3. Gas impurities measurements

Helium and hydrogen gas impurity measurements were conducted on multiple specimens from each test sample by mass spectrometry. The specimens were taken from a cross-sectional section of each tube that included the entire fracture surface. For the hydrogen measurements, the specimens were prepared by cutting sections from the tube segment along the original longitudinal axis, thereby maintaining an approximately constant amount of fracture surface per unit mass for each

analyzed piece. Specimens for both helium and hydrogen measurement were rinsed in acetone and then air dried prior to analysis. All the specimens for helium analysis were first etched to remove recoil or other surface effects. Etch depth range from approximately 15–45 μm, based on the mass of material that was removed. Details of the helium and hydrogen analysis systems has been given elsewhere [18,19].

Most of the specimens for hydrogen analysis were not etched in order to avoid possible interferences from hydrogen pickup from the etching process. However, during sample preparation it was observed that all the irradiated samples had a 'bluish' surface layer on the outside of the tube segment. This layer, which has been noted previously in proton beam experiments at PSI is believed to be an oxide which could inhibit the outflow of hydrogen, and thus could influence the retention of hydrogen generated in the F82H material from the proton beam. Although not visible, it is assumed that a similar oxide layer existed on the inside surface of the tube segments. As a result, selected specimens were also prepared with varying amounts of surface removed in order to determine the depth profile of the retained hydrogen.

The gas analysis results are presented in Table 4, with the associated dose of each measured sample. For the helium samples, the dose corresponds to the complete original sample before cutting and etching. For the hydrogen samples, however, the doses were determined for selected specimens from measurements of the ^{54}Mn specific activity. This was done to correct for possible gradients in the proton dose across the tube section. The

concentration data in Table 4 have been plotted as a function of the dose in Fig. 6. As expected, the helium data are very consistent and show very little scatter, and indicate an average helium production rate of 125 appm/dpa.

An initial set of hydrogen measurements were conducted on specimens with the original surface intact. These data showed a reasonably consistent increase with increasing dpa (see Fig. 6), except for two samples, I15I5 and I16I11, which showed relatively high concentrations. To examine for possible effects from the observed surface oxide layer, additional analyses were conducted on specimens which had varying depths of surface material removed by either acid etching or micro-sandblasting or both. These specimens are identified in Table 4. Etching was performed with room-temperature aqua-regia (3HCl + 1HNO$_3$) for approximately 1 min. Etch depth was ∼5 μm from each surface as determined from mass loss. Sandblasting was done with 50 μm alumina powder, with a surface removal depth estimated to range from ∼1 to ∼2 μm depending on the assumed density of the oxide. In each case, i.e., etching or sandblasting, the surface layer was not visible after the procedure.

The hydrogen measured in the etched specimens of I16I5 and I16I11, as well as in etched specimens of I16I7, I16I9, and I16T38, was significantly lower than for the un-etched material, and represents the hydrogen remaining in the bulk material (as the etching was ∼5 μm on each surface). The hydrogen measured in the sandblasted specimens from I16I8, which had ∼1–2 μm removed from their surfaces, represents the hydrogen accumulated in the bulk plus in the outside layers of the
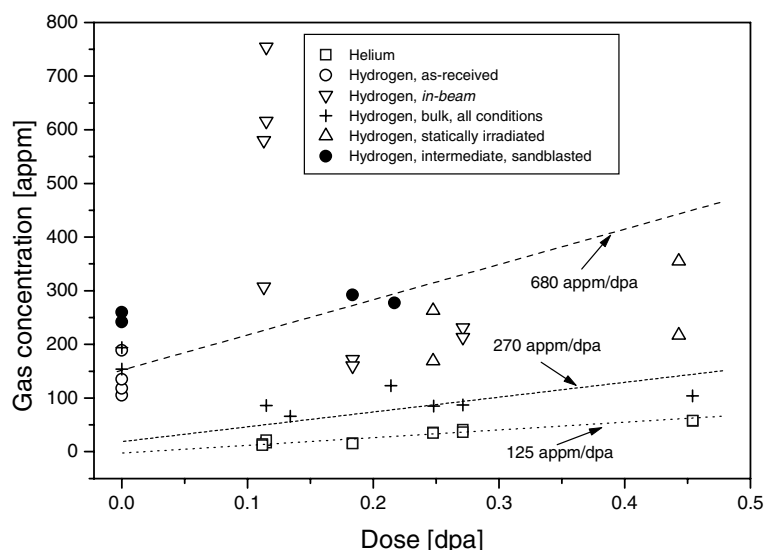

Fig. 6. Helium and hydrogen gas concentrations found in the specimens as a function of the dose. The helium data points show little scatter whereas the hydrogen dataset is more dispersed due to variability in the trapping of the hydrogen gas in the material.

specimen just underneath the oxide. This corresponds to an intermediate case were some of the outside layer is still present. The specimen of I16I8 which was sandblasted and then etched lost a total of about 6–7 μm. The measured hydrogen in this sample was consistent with the results for the bulk material. It should be noted that the zero dpa hydrogen values indicated in Table 4 (N16I4 and N16I10) and shown in Fig. 6 are for the as-received material. These samples were never heated to 300 °C.

Considering the relatively large scatter in the results and the apparently strong influence of the surface oxide, it was decided to limit the acceptable data to those falling between a lower limit representing the bulk hydrogen content and a higher limit representing the bulk + outside layer immediately under the oxide. These limits are shown in Fig. 6. The lower bound production rate is estimated at 270 appm/dpa and the higher bound at 680 appm/dpa.

4. Discussion

The *in-beam* fatigue results obtained from fission neutrons or from low energy ions in austenitic and FM steels [3–5,7,8,20] all suggest two main results. First, the *in-beam* fatigue in these materials strongly reduces irradiation hardening. As the cycles accumulate, so does the dose but the associated total stress range is not increasing. If it does, it is only after a very high number of cycles or if the imposed frequency is low or during hold times. Second, the fatigue life of the post-irradiation tested specimens represent a lower limit for the endurance of the *in-beam* specimens. The fatigue life of the *in-beam* specimens was generally longer than the life of the post-irradiation tested specimens, and when tested at a high imposed strain range, the life was comparable to the life of the unirradiated specimens.

These two main results can be understood in terms of the damage ratio $m = \dot{D}/\dot{\varepsilon}$, where $\dot{D}$ is the dose rate and $\dot{\varepsilon}$ the strain rate [11]. If m is large then the fatigue damage will be dominated by the cascade defects from the PKA's and the resulting cyclic hardening from the irradiation substructure evolution. If m is small then the damage will be controlled by classical fatigue damage, whereas the mobile dislocations absorb most of the point defects generated and are slowed down during the process. This absorption process produces viscous drag on the dislocations. This viscous drag should also have a detrimental effect on crack propagation, but smaller than the effect produced in the case of dislocations interacting with stable defects.

The above approach holds also for the 590 MeV proton irradiated specimens, as illustrated by the two experiments I16I11 and I16I7. I16I7 was tested at a low frequency and thus has a high damage ratio, showed cyclic hardening at the end of life, whereas the associated total plastic strain is significantly reduced. For comparison, I16I11 tested at high frequency behaves similar to the unirradiated specimen N16F2 (see Figs. 1 and 3). It seems that at $m = 3 \times 10^{-3}$ (I16I11) short range defects and loops do not form in significant quantity, but that at $m = 8 \times 10^{-3}$ (I16I7) an irradiation substructure with associated irradiation hardening is slowly forming. As was the case for I16I7, despite its short duration, the experiment with tension hold times I16I8, shows some cyclic hardening and a reduction of the total plastic strain, suggesting that the dislocations are interacting with the defects. Nevertheless the observed reduction in life (see N_a in Table 2) seems too strong as compared with the effects on strength and strain. The same applies for I16I11, which behaves mechanically like the unirradiated specimen, but has a significantly shorter life, even shorter than the post-irradiation tested specimen. Therefore, it is suspected that another damage component is acting during the *in-beam* fatigue with high energy protons.

Our measurements show that helium is introduced by the protons at a rate of 125 appm/dpa in the bulk, which is in agreement with the HETC calculation [13]. Helium is present in too small quantities (up to 41 appm, Table 4), however, to produce any significant effect on the mechanical properties [21]. As shown in Table 4 and Fig. 6, hydrogen is also generated by the high energy protons in the steel, at rates estimated between 270 and 680 appm/dpa. These storage rates compare well with the HETC prediction of 956 appm/dpa, taking into account that about 30% is lost due to the high recoil energy of the produced hydrogen and that some of the generated hydrogen is likely lost from the specimen by diffusion before being trapped in the microstructure. Despite the relatively high temperature of the experiments (300 °C), we can conclude that hydrogen was stored in the material and was located mostly underneath the surface. It seems that the oxide layers formed during the irradiation act as barrier and reduce the quantity of hydrogen leaving the specimens. The quantity of stored hydrogen does not seem to depend on whether the specimen was irradiated *in-beam* or statically.

The results from the fractographs indicate a high density of microcracks at the lath boundaries, for all observed conditions. Only a few secondary cracks are observed on the surface. In F82H, most probably, many cracks nucleate in the bulk at the lath boundaries. This is because those boundaries are weak due to the presence of precipitates.

Our results indicate that the embrittlement is stronger in the in situ irradiated specimens as compared to the post-irradiation tested specimen. During fatigue in FM steels, subgrains having very low internal dislocation densities are formed in the martensite lathes [17]. The amount of plastic deformation, and the number of

cycles, are the controlling parameters. The higher they are, the more of the material will be transformed in cell structure. The process is slowed down in irradiated material where it will take more cycles to form the subgrains. In the in situ tested material, subgrains are formed relatively rapidly. During irradiation with concurrent deformation, atomic hydrogen is fed continuously into the bulk of those subgrains and can be easily transported by the moving dislocations to the singularities of the microstructure [22]. The sink strength of the hydrogen traps is enhanced, whereas in the post-irradiation tested specimen, the hydrogen will mostly be collected in the interior of the lathes, at the high density dislocation network. Therefore, for the parameters of our experiment, and for F82H, the damage is stronger in the in-beam specimens as compared to the post-irradiation tested specimen.

The damaging potential of hydrogen in FM steels has been previously analysed and demonstrated in fatigue and tensile experiments [23–26]. It is well known that the degree of hydrogen embrittlement increases as the strain rate decreases and that the negative effect of hydrogen is exacerbated by hold times during the fatigue cycle [24]. This is also demonstrated in this work by the dramatic effect of 2 min hold times on the behaviour of I16I8 and the presence of numerous brittle features in the fractographs of this particular specimen. Therefore, the additional damage component producing the dramatic reduction of lives observed during 590 MeV p *in-beam* fatigue is probably hydrogen. Fission neutrons or low energy ions do not generate hydrogen. Experiments using these types of particles consequently show less effects in terms of embrittlement.

5. Conclusions

A batch of F82H steel specimens have been fatigued in a beam of 590 MeV protons, at a total controlled strain range near 0.8%, at 300 °C, and doses up to 0.3 dpa. The principal results are as follows:

- The *in-beam* fatigue results show a strong dependence on the mechanical and irradiation parameters imposed, as described by a damage ratio parameter $m = \dot{D}/\dot{\varepsilon}$, where $\dot{D}$ is the dose rate and $\dot{\varepsilon}$ the strain rate.
- The post-irradiation tested specimen shows the strongest cyclic softening. The *in-beam* specimen have the lowest cyclic softening. Classical irradiation hardening is almost suppressed in the *in-beam* specimens.
- The total plastic strain is reduced during tests at low frequency, whereas the life is also reduced.
- The fatigue lives of the *in-beam* specimens are clearly shorter as compared to the post-irradiation tested and unirradiated specimens. The introduction of 2

min hold times has a dramatic effect on fatigue life and represents the worst case.
- Crack initiation is found to occur predominantly at the lath interfaces, for all tested conditions.
- The gas impurity measurements performed on the specimens indicate that helium (15–40 appm) and hydrogen (80–300 appm) are retained in the microstructure. Since helium is known to be harmless at low levels, hydrogen is suspected to be a main contributor to the observed embrittlement.

F82H steel seems to be sensitive to hydrogen fatigue embrittlement at medium temperatures. The prospect of using similar materials in the first wall of fusion reactors where hydrogen will be generated [25] or in spallation source windows, will require further research, if the components are fatigued during irradiation.

Acknowledgements

References

[1] G.S. Bauer, M. Salvatores, G. Heusener, J. Nucl. Mater. 296 (2001) 17.
[2] L.K. Mansur et al., J. Nucl. Mater. 296 (2001) 1.
[3] W. Vandermeulen et al., J. Nucl. Mater. 183 (1991) 57.
[4] R.V. Nieuwenhove, F. Moons, In-Pile AISI 316L Low Cycle Fatigue, SCK-CEN, 1994.
[5] P. Fenici, J. Nucl. Mater. 155–157 (1988) 963.
[6] P. Fenici, S. Suolang, J. Nucl. Mater. 191–194 (1992) 1408.
[7] R. Scholz, R. Mueller, J. Nucl. Mater. 258–263 (1998) 1600.
[8] R. Scholz, R. Mueller, J. Nucl. Mater. 233–237 (1996) 169.
[9] J. Bertsch, R. Lindau, A. Möslang, J. Nucl. Mater. 233–237 (1996) 276.
[10] R. Lindau, A. Möslang, J. Nucl. Mater. 212–215 (1994) 599.
[11] P. Marmy, J. Nucl. Mater. 212–215 (1994) 594.
[12] W.V. Green, M.P. Victoria, S.L. Green, J. Nucl. Mater. 133&134 (1985) 58.
[13] S. Proenecke, Impurity calculation from HETC in ferritic steel from 600 MeV protons, 1990.
[14] P. Marmy, Plasma Devices Oper. 4 (1996) 211.
[15] P. Marmy, In-situ Fatigue Properties of MANET steels in a 590 MeV Proton Beam, Centre de Recherches en Physique des Plasmas, CH-1015 Lausanne, 2003.
[16] R. Schäublin, P. Spätig, M. Victoria, J. Nucl. Mater. 258–263 (1998) 1178.
[17] P. Marmy, Y. Ruan, M. Victoria, J. Nucl. Mater. 179–181 (1991) 697.

[18] H. Farrar, B. Oliver, J. Vac. Sci. Technol. A 4 (1986) 1740.

[19] B.M. Oliver et al., J. Nucl. Mater. 283–287 (2001) 1006.

[20] A. Möslang et al., Fusion Technol. (1992) 1439.

[21] H. Schroeder, H. Ullmaier, J. Nucl. Mater. 179–181 (1991) 118.

[22] J.P. Hirth, Metall. Trans. A 11A (1980) 861.

[23] M. Beghini et al., J. Nucl. Mater. 258–263 (1998) 1295.

[24] J.I. Shakib et al., J. Nucl. Mater. 212–215 (1994) 579.

[25] P. Jung, J. Nucl. Mater. 258–263 (1998) 124.

[26] P. Jung, C. Liu, J. Chen, J. Nucl. Mater. 296 (2001) 165.